Int. J. Electrochem. Sci., 8 **(2013)** 11615 - 11623

International Journal of ELECTROCHEMICAL SCIENCE
www.electrochemsci.org

Effects of Platinum Doping on the Photoelectrochemical Properties of Fe_2O_3 Electrodes

Ya-Ping Hsu[1], *Sheng-Wei Lee*[2], *Jeng-Kuei Chang*[1,2], *Chung-Jen Tseng*[1,*], *Kan-Rong Lee*[1], *Chih-Hao Wang*[1]

[1]Department of Mechanical Engineering, National Central University, Jhongli, Taiwan
[2]Institute of Materials Science and Engineering, National Central University, Jhongli, Taiwan
[*]E-mail: cjtseng@ncu.edu.tw

Received: 8 May 2013 / *Accepted:* 12 June 2013 / *Published:* 20 August 2013

The effects of platinum (Pt) doping on the structure and photoelectrochemical properties of Fe_2O_3 electrodes have been investigated. The Pt-doped Fe_2O_3 electrodes were prepared by sol-gel and spin coated on fluorine-tin-oxide coated glass substrate. Influences of dopant concentration on material properties and photoelectrochemical characteristics were examined. Results of XRD and XPS showed that α-Fe_2O_3 can be obtained using 500 ^{o}C annealing in air. The band gaps of the samples obtained from reflectance and transmittance spectra measurement were found to vary from 1.98 to 2.03 eV. The flat band potentials of the samples were obtained from the Mott-Schottky analysis and found to be in the range of -0.135 V to -0.6 V. The maximum photocurrent density of undoped and 0.1 at.% Pt-doped Fe_2O_3 electrodes was 0.5 mA/cm^2 and 0.7 mA/cm^2 under a 300 W Xe lamp system, respectively. The good photoelectrochemical results of the Pt-doped Fe_2O_3 electrode warrant further investigation for broader applications in the future.

Keywords: Fe_2O_3, Pt-doping, Sol-gel process, Photoelectrochemical method, thin films

1. INTRODUCTION

Hydrogen is a promising energy carrier for the future [1]. It can be produced by many methods from a variety of sources. One promising method is the photoelectrochemical (PEC) splitting of water using solar irradiation [2-7]. The n-type titanium dioxide (TiO_2) is a promising substrate for photogeneration of hydrogen from water, and many works have been done in modifying the microstructure of the material to increase the energy conversion efficiency [8]. Other semiconductors, such as Fe_2O_3, WO_3, and ZnO, have also attracted much attention.

Hematite (α-Fe_2O_3) has emerged as a promising photo-electrode material due to its significant light absorption, chemical stability in aqueous environments, and ample abundance. The energy band gap of α-Fe_2O_3 is about 2.1 eV, enabling better utilization of the solar energy for water splitting than using TiO_2 electrodes. Good stability of the α-Fe_2O_3 electrode in alkaline solution was discussed by Kennedy and Frese [9]. Aroutiounian et al. [10-11] have reported the hopping mechanisms of various doping metals (Nb, Sn, Ta) with iron oxide powder in photoelectrochemical systems. The results indicated that photon-electron conversion efficiency of Nb-doped α-Fe_2O_3 thin films was 26 % under illumination conditions of simulated Air Mass (AM) 1.5 solar irradiation [12]. The photoelectrochemical properties of Cu and Zn doped α-Fe_2O_3 thin films was reported by Satsangi et al. [13]. They found that 1.5 at% Zn doped α-Fe_2O_3 exhibited the highest photocurrent density, 87.9 $\mu A/cm^2$ at 0.6 V vs. SCE (pH=13). The photocurrent responses of Si-doped α-Fe_2O_3 were reported by Flavio et al. [14]. By doping silicon, the photocurrent density increased due to enhancement of (110) crystallization. The maximum photocurrent density of Si-doped α-Fe_2O_3 at 0.5 V vs. Ag/AgCl (pH=13.6) in 1M NaOH was approximately 60 $\mu A/cm^2$.

Luo et al. [15] used WO_3/Fe_2O_3 composite thin film to enhance photocurrent density. They proposed that the photo-generated electrons could transfer more easily in WO_3/Fe_2O_3 than in WO_3 or Fe_2O_3 alone because the conduction band of WO_3 is higher than that of Fe_2O_3. Later, Wang et al. [16] prepared $SrTiO_3/Fe_2O_3$ composite photoanode by spin-coating. They found that the photocurrent of the $SrTiO_3$/α-Fe_2O_3 heterojunction were higher than that of the single $SrTiO_3$ or α-Fe_2O_3 film, particularly under visible light irradiation. Sartoretti et al. [17] prepared Ti-doped iron oxide thin film by spray pyrolysis. They found that doping Ti increases the conductivity and stability of iron oxide film. On the other hand, doping Ni or In reduces the photocurrent density.

In this study we investigate the effect of Pt doping on the structures and optical and PEC properties of α-Fe_2O_3 thin film photoanode.

2. EXPERIMENTAL METHODS

2.1. Preparation of electrodes

Un-doped Fe_2O_3 and Pt-doped Fe_2O_3 were prepared by sol-gel spin-coating on fluorine doped tin oxide (FTO) glasses. The substrates were cleaned with alcohol, acetone, and isopropanol before each coating. The precursor of reaction solvent was $FeCl_3 \cdot 6H_2O$ (0.5 M), adjusted to a volume ratio of 36:1:1 mixture of $(CH_3)_2CHOH$, $HOCH_2CH_2OH$, and HCl. Platinum was added from different $PtC1_6H_2 \cdot 6H_2O$. The molar ratio of Pt to Fe was controlled at 0.1 %, 0.5%, 1.0%, and 1.5 %. Dust and other suspended impurities were removed from the solution by filtering through a 0.2 μm syringe filter. The spin speed was kept at 5000 rpm for 20 seconds. All films were heated in air at 250°C for evaporation of the solvent, and then heat treated at 500°C for 2 hours.

2.2. Characterization of electrodes

The morphology of samples was observed using field emission scanning electron microscope (FE-SEM, JEOL, JSM-7401F). The crystal structure of samples was measured using an X-ray diffractometer (XRD, Shimadzu, XRD-6000 X) with CuKα (λ = 1.5418 Å) radiation in the 2θ range of 20-65°. The scan rate was 5 °/min.

The optical characteristic of samples was measured by UV-Vis spectrophotometer with an integrating sphere (JASCO, V-670) and resolution of 1 nm. After obtaining the transmittance, T and reflectance, R of the Fe_2O_3 films, the absorption coefficient (α) can be calculated from [18]:

$$\alpha = \frac{1}{d}\left(\ln\frac{1-R}{T}\right) \qquad (1)$$

where d (nm) is the thickness of the film. The energy band gap, E_g can then be determined from the following equation [19]:

$$\alpha h v = A\left(hv - E_g\right)^n \qquad (2)$$

where $h\upsilon$ is the incident photo energy, A is a constant. n = 1/2 indicates direct allowed transition, and n = 2 indicates indirect allowed transition.

Mott-Schottky (M-S) measurements for the evaluation of the flat-band potentials of samples were performed using a potentiostat (Autolab, ECO CHEMIE, PGSTAT302) with a frequency response analyzer. The applied potentials were set in the range of -0.8 to + 0.2 V (versus Ag/AgCl reference electrode). The frequency of the Mott-Schottky plots was set at 1 kHz in this study. The flat-band potential (E_{fb}) for Fe_2O_3 thin films can be determined using [20]:

$$\frac{1}{C^2} = \left[\frac{2}{q\varepsilon\varepsilon_0 N_D}\right]\left[E - E_{fb} - \left(\frac{kT}{q}\right)\right] \qquad (3)$$

where C, q, ε_0, N_D, and E_{fb} are capacitance, the electron charge, permittivity in vacuum, donor carrier density and flat-band potential of the semiconductor, respectively. The flat-band potentials of samples can be obtained from the intersection of the C^{-2} vs. applied potential, E, plot.

Furthermore, the PEC performances of films were measured in a standard three-electrode system consisting of a Fe_2O_3 sample as the working electrode, a Pt plate (~1 × 1 cm^2) as the counter electrode, Ag/AgCl as the reference electrode, and Na_2S (0.35 M) and K_2SO_3 (0.25 M) as the aqueous electrolyte (pH value = 13). The electrolyte was prepared using double deionized water and degassed by purging with nitrogen gas before each experiment. The photocurrent density of films, as a function of applied voltage, was varied from - 0.5 V to + 1.0 V vs. Ag/AgCl reference electrode (scan rate = 0.05 V/s) and using a 300 W solar simulator (Newport-Oriel Instruments, Model: 91160-1000) with AM 1.5 filter as a light source.

3. RESULTS AND DISCUSSION

The crystal structures of the un-doped and Pt-doped (0.1、0.5、1.0、1.5 at%) Fe_2O_3 after sol-gel spin-coating and annealing are shown in Figure 1. The intensity of diffractive peak corresponding to α-Fe_2O_3 crystallinity increases with the content of Pt doped. The grain size can be obtained with the aid of Scherrer’s equation

$$D = \frac{0.9\lambda}{\beta\cos\theta} \qquad (4)$$

where *D*, λ, β, and θ are the mean grain size, X-ray wavelength, the full width at half maximum (FWHM) of the diffraction peak, and the Bragg angle, respectively.

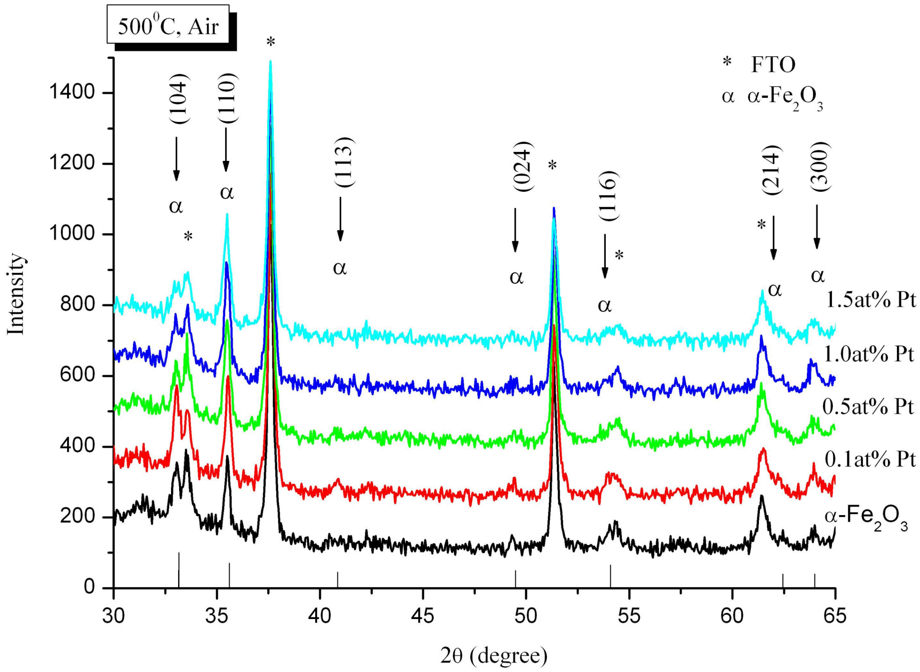

Figure 1. X-ray diffraction results of undoped and Pt-doped Fe_2O_3 thin films.

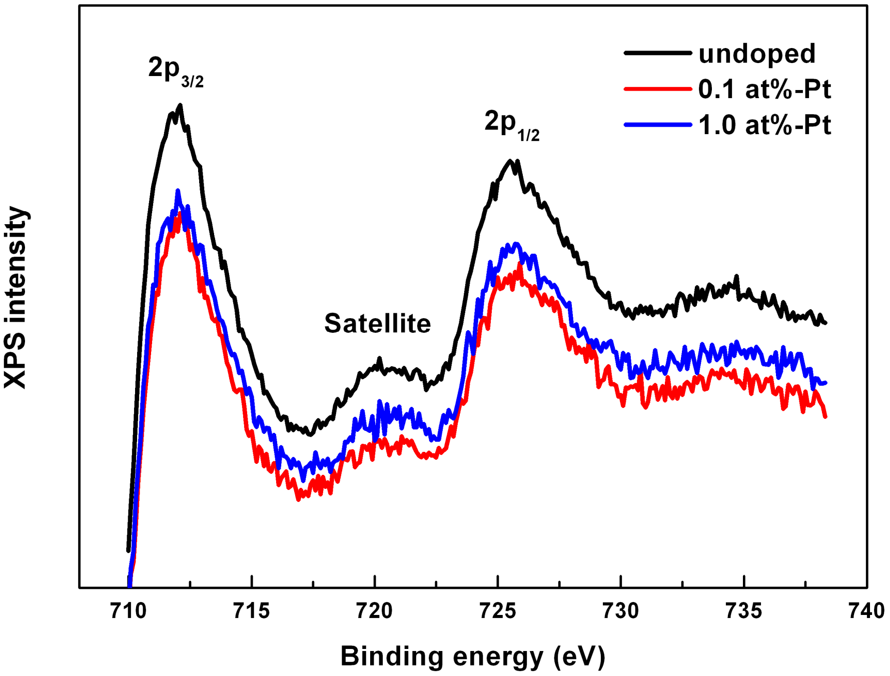

Figure 2. XPS Fe 2p orbital spectra of Fe_2O_3 thin films.

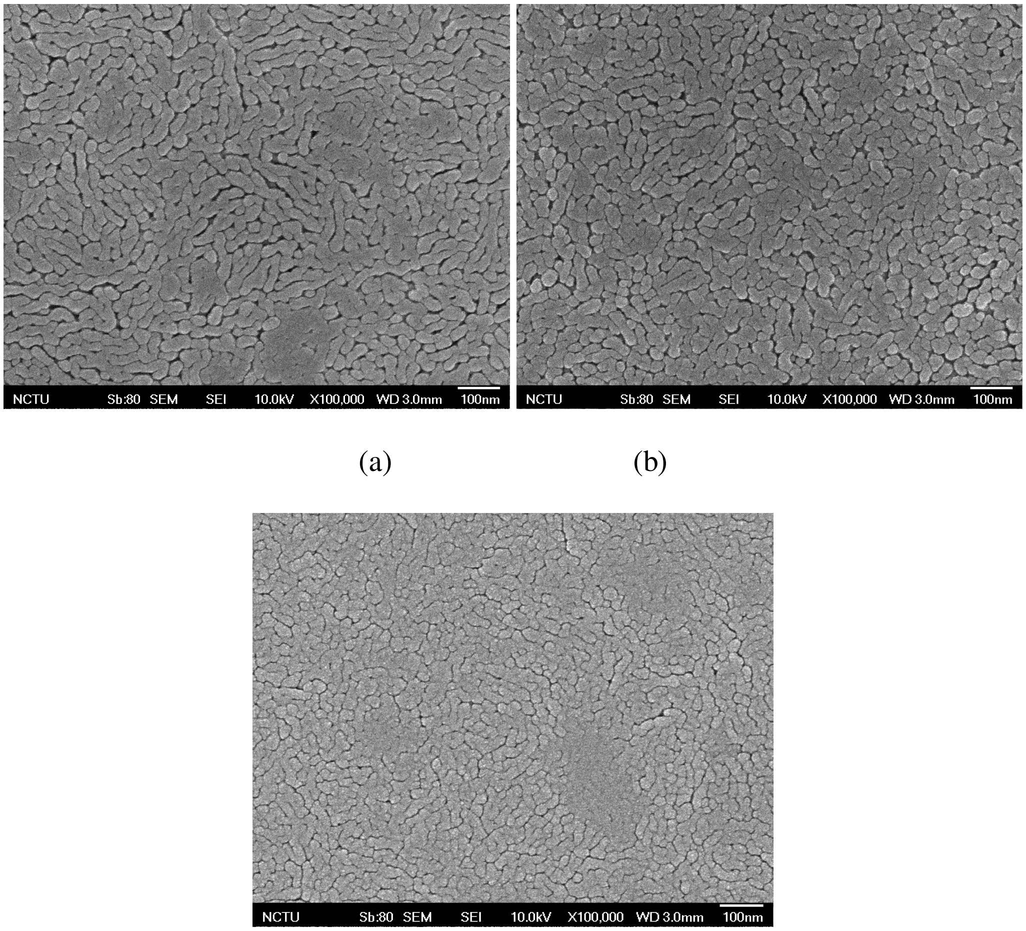

(a) (b)

(c)

Figure 3. FE-SEM images of Fe_2O_3 thin films (a) undoped (b) 0.1 at % Pt doped and (c) 1.5 at % Pt doped.

From this equation, the grain size of the undoped sample calculated from the (110) peak was found to be 64 nm. The grain size decreases from 56, 52, 50, to 44nm as the amount of Pt doped increasing from 0.1, 0.5, 1.0, 1.5 at%. Figure 2 shows the XPS results of un-doped and Pt-doped Fe_2O_3 thin films. The $2p_{3/2}$ and $2p_{1/2}$ signals were observed.

Table 1. Values of physical properties for Pt-doped α-Fe_2O_3 thin films.

Atmosphere	Pt (at%)	Thickness (nm)	E_g (eV)	E_{fb} (V vs. Ag/AgCl)	Conduction type
Air	0 at%	228.4	2.03	-0.600	n
	0.1 at%	267.5	2.02	-0.321	n
	0.5 at%	201.5	2.00	-0.235	n
	1.0 at%	270.3	1.99	-0.155	n
	1.5 at%	167.9	1.98	-0.135	n

The fact that the satellite peak is closer to $2p_{1/2}$ confirms the samples are pure iron oxide of alpha phase [21]. The small amount of Pt doping does not alter the chemical state of α-Fe_2O_3 thin film. The thickness of the samples was measured by α-step and found to range from 168 to 268 nm as shown in Table 1. The FE-SEM images for the un-doped and Pt-doped α-Fe_2O_3 thin films are shown in Figure 3. They show worm-like grains.

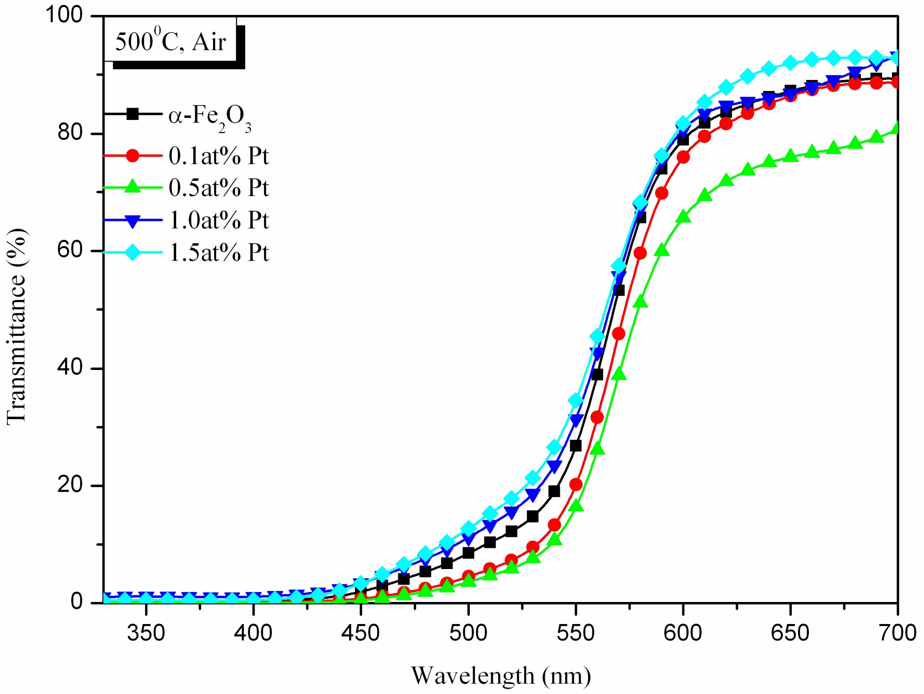

Figure 4. Transmittance spectra of Fe_2O_3 films.

Figure 4 shows transmittance spectrum measured at room temperature by ultraviolet-visible spectrometer. These films are highly transparent in the range from 580 nm to 700 nm. A similar result was also observed by Ismail et al [22]. The $(\alpha h\nu)^{1/2}$ vs. $h\nu$ plot is shown in Figure 5. The band gap of the samples can be obtained from extrapolating the linear portions of the respective curve to $(\alpha h\nu)^{1/2} = 0$. The band gap of the various Pt-doped Fe_2O_3 films was found to be in the range of 1.98-2.03 eV. We observed that the band gap is slightly red-shifted by increasing Pt doping concentration. Figure 6 shows the Mott-Schottky plots for the samples. The flat band potentials were obtained by extrapolating the curves to the intercept with $C^{-2} = 0$. The positive slope of the Mott-Schottky plot confirms the n-type conductivity of the samples. The flat band potential evaluated from Mott–Schottky plots are in the range from -0.135 to -0.6 V vs. Ag/AgCl electrode, and increases with the amount of Pt doped. The flat band potential shifting toward positive is probably due to the electronic structure change with platinum doped in Fe_2O_3 films. Values of band gaps and flat band potentials of the samples are also summarized in Table 1.

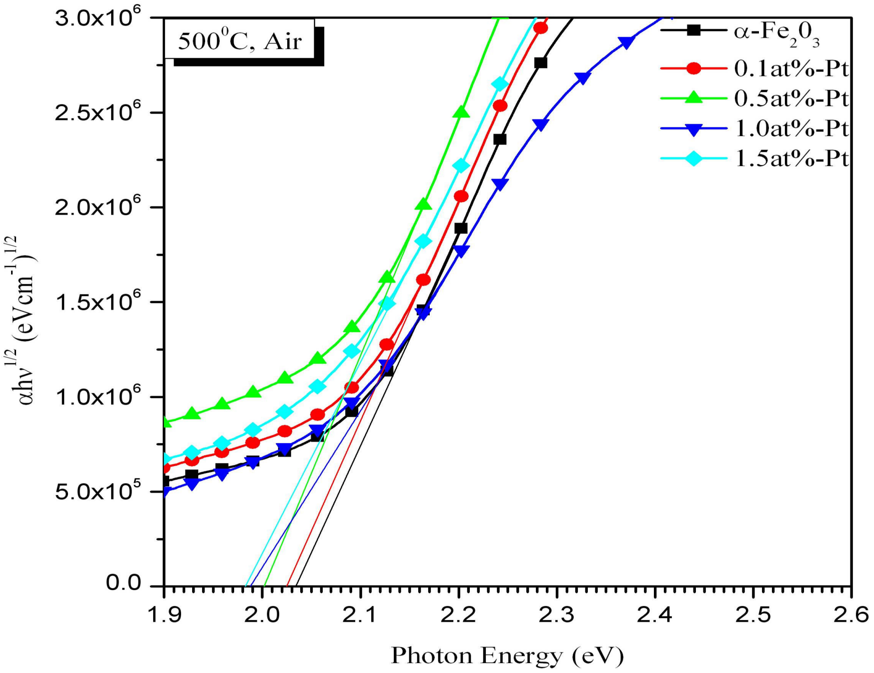

Figure 5. Plots of $(\alpha h\nu)^{1/2}$ vs. hν of doped and undoped films.

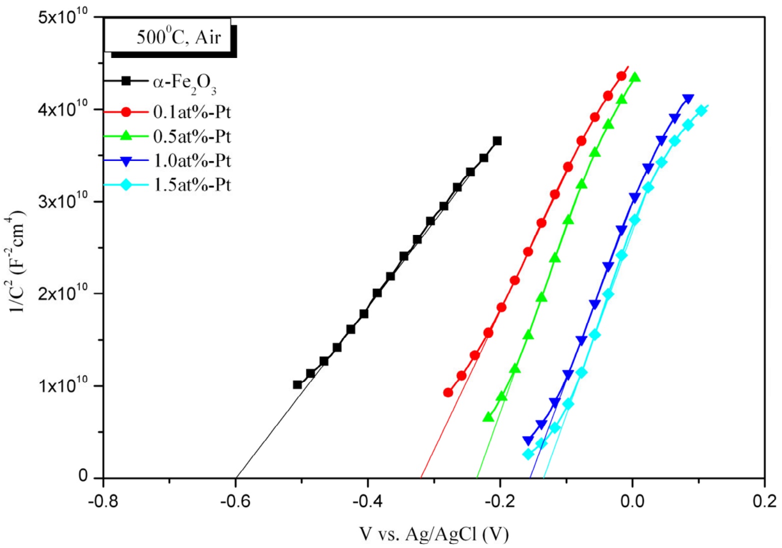

Figure 6. Mott-Schottky plots of doped and undoped films in 0.5 M K_2SO_3 + NaOH as the electrolyte (pH =13).

Figure 7 demonstrates photocurrent density as a function of applied potential (vs. Ag/AgCl) of the un-doped and Pt-doped Fe_2O_3 samples in 0.5 M K_2SO_3 + NaOH (pH = 13) electrolyte solution. It is interesting to note that the onset voltage of photocurrent of Fe_2O_3 samples shifts toward more positive with increasing concentration of Pt-doping, consistent with the Mott-Schottky measurement results. It can be seen that 0.1 at% Pt-doped Fe_2O_3 exhibited the maximum photocurrent density value of 0.7 mA/cm^2.

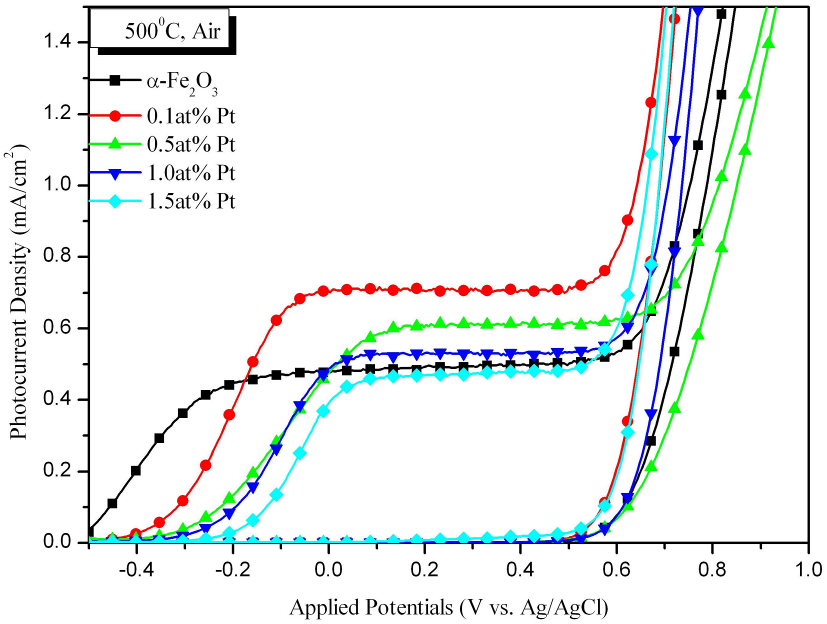

Figure 7. Photocurrent density - applied voltages plots of samples under 300 W solar simulators (AM 1.5G, 100 mW/cm^2, 25°C).

Compared to the maximum photocurrent density of 0.5 mA/cm^2 of the un-doped sample, the enhancement is about 40 %. The addition of Pt increases electronic conduction. Adding Pt also increases crystallinity of Fe_2O_3 as evidenced by the intensity of the (110) peak in XRD results that helps charge carriers transfer more effectively. However, the photocurrent density decreases as the amount of Pt is further increased. As shown previously, the grain size decreases with increase Pt concentration. Therefore, the increased number of grain boundaries raises the recombination rate of photogenerated carriers.

4. CONCLUSIONS

We have successfully deposited platinum-doped Fe_2O_3 films on FTO glasses by sol-gel spin-coating technique. The crystallite grain sizes are found to vary from 44 nm to 64 nm by XRD analyses. FESEM study showed worm-like morphology with nearly uniform grain distribution. The energy band gaps are found to vary from 1.98 eV to 2.03 eV. The flat band potentials are in the range between -0.135 V and -0.6 V vs. Ag/AgCl electrode. The 0.1 at% Pt-doped sample has the maximum photocurrent density of 0.7 mA/cm^2.

References

1. M. Momirlana, T.N. Veziroglu, *Int. J. Hydrogen Energy* 30 (2005) 795.
2. C.-L. Tseng, C.-J. Tseng, J.-C. Chen, *Int. J. Hydrogen Energy* 35 (2010) 2781.
3. C.-H. Wang, K.-W. Cheng, C.-J. Tseng, *Sol. Energy Mater. Sol. Cells* 95 (2011) 453.
4. C.-J. Tseng, C.-H. Wang, K.-W. Cheng, *Sol. Energy Mater. Sol. Cells* 96 (2012) 33.
5. Z. Zhang, M.F. Hossain, T. Takahashi, *Int. J. Hydrogen Energy* 35 (2010) 8528.
6. C.-J. Tseng, C.-L. Tseng, *Int. J. Hydrogen Energy* 36 (2011) 6510.
7. A. Fujishima, K. Honda, *Nature* 238 (1972) 37.
8. Z. Zhang, P. Wang, *Energy Environ. Sci.* 5 (2012) 6506.
9. J.H. Kennedy, K.W. Frese Jr, *J. Electrochem. Soc.* 125 (1978) 709.
10. V.M. Aroutiounian, V.M. Arakelyan, G.E. Shahnazaryan, H.R. Hovhannisyan, H. Wang, J.A. Turner, *Solar Energy* 81 (2007) 1369.
11. V.M. Aroutiounian, V.M. Arakelyan, G.E. Shahnazaryan, G.M. Stepanyan, J.A. Turner, O. Khaselev, *Int. J. Hydrogen Energy* 27 (2002) 33.
12. http://rredc.nrel.gov/solar/spectra/am1.5/.
13. V.R. Satsangi, S. Kumari, A.P. Singh, R. Shrivastav, S. Dass, *Int. J. Hydrogen Energy* 33 (2008) 312.
14. L.S. Flavio, P.L. Kirian, A.P. Nascente, R.L. Edson, *Sol. Energy Mater. Sol. Cells* 93 (2009) 362.
15. W. Luo, T. Yu, Y. Wang, Z. Li, J. Ye, Z. Zou, *J. Phys. D: Appl. Phys.* 40 (2007) 1091.
16. Y. Wang, T. Yu, X. Chen, H. Zhang, S. Ouyang, Z. Li, J. Ye, Z. Zou, *J. Phys. D: Appl. Phys.* 40 (2007) 3925.
17. C.J. Sartoretti, B.D. Alexander, R. Solarska, I.A. Rutkowska, J. Augustynski, *J. Phys. Chem. B* 109 (2005) 13685.
18. J.C. Manifacier, M.D. Murcia, J.P. Fillard, E. Vicario, *Thin Solid Films* 41 (1977) 127.
19. M.S. Selim, A. Sawaby, Z.S.E. Mandoud, *Mater. Res. Bull.* 35 (2000) 2123.
20. S. Kumari, C. Tripathi, A. P. Singh, D. Chauhan, R. Shrivastav, S. Dass, V.R. Satsangi, *Curr. Sci.* 91 (2006) 1062.
21. S. Gota, E. Guiot, M. Henriot, G.S. Martine, *Phys. Rev. B* 60 (1999) 14387.
22. R. A. Ismail, Y. Najim, M. Ouda, *J. Surf. Sci. Nanotech.* 6 (2008) 96.